CLM-P699

CLM-P699

UKAEA

Preprint

SURFACE CLADDING BY MULTIKILOWATT LASER

J. H. P. C. MEGAW
A. S. BRANSDEN
D. N. H. TRAFFORD
T. BELL

CULHAM LABORATORY
Abingdon Oxfordshire

1983

SURFACE CLADDING BY MULTIKILOWATT LASER

by

J.H.P.C. Megaw*, A.S. Bransden*, D.N.H. Trafford** and T. Bell***

Abstract

This work, which was carried out using an industrially-rated 5kW laser (CL5) at Culham Laboratory, had the objective of assessing a number of selected laser cladding operations. Using defocused beam, preplaced powder and careful gas shielding, four cladding/substrate combinations have been investigated. These were chromium carbide on nickel alloy, Stellite on cast iron or steel, and silicon on aluminium alloy. Operating regimes (in terms of applied power density and interaction time) were investigated and compared for all four. Aspects such as porosity, cracking, dilution, ductility and post-deposition heat treatment received attention. In addition, very encouraging results of wear performance were seen in the chromium carbide and silicon coatings.

Paper to be published in Proceedings of 3rd International Colloquium on Welding & Melting by Electron & Laser Beams (CISFFEL), Lyon, September 1983. Colloquium organised by le Commissariat a l'Energie Atomique/l'Institute de Soudure.

* UKAEA Culham Laboratory, Abingdon, Oxfordshire, OX14 3DB, UK.
** Dept. of Metallurgy, University of Liverpool, PO Box 147, L69 3BX, UK.
*** Dept. of Metallurgy and Materials, University of Birmingham, PO Box 363, B15 2TT, UK.

1. INTRODUCTION

The aim of this work was to develop a relatively broad base of experience which would facilitate subsequent investigations of specific component applications. A (metallurgically) wide range of coating/substrate combinations was studied and processing conditions were compared. The combinations were chosen to be representative of: carbide coatings; cobalt-base alloy cladding; silicon strengthening of aluminium alloy. In each combination, investigations were made of metallurgical and physical properties such as porosity, cracking, dilution, ductility and wear performance. Combination A, in contrast to previously reported carbide studies (1)(2)(3), utilised a commercial powder of chromium carbide (85%) in Ni/Cr (4:1) on Ni alloy (43.5% Ni, 34% Fe, 16% Cr) and the wear performance of the laser deposited layer was compared with that of a flame-sprayed coating. In combination B, the choice of cast-iron (Grade 17 Meehanite G.C.) substrate for the cobalt-base alloy (Stellite Alloy No.6) cladding was considerably more challenging than earlier work featuring Nimonics (4)(5). Problems studied included porosity, but ultrasonic vibration of the workpiece, reported beneficial in other work (6), was rejected as impracticable here because of likely component mass. Deposition of Stellite 6 on structural steel (BS4360 Grade 43A), combination C, was briefly investigated. Finally, (combination D) the work on strengthening aluminium with silicon powder utilised a non heat-treatable 4½%Mg alloy (BS1474-5083), rather than the Al-Si eutectic compositions of previous studies (2)(7), and furthermore it featured measurements of wear resistance.

2. APPARATUS & PROCEDURE

The laser treatment utilised the Culham Laboratory 5kW industrial CO_2 laser Model CL5. In contrast to earlier transformation hardening studies(8), beam rastering was not used and samples were traversed beneath the stationary, downward-going beam at different distances from focus. The annular cross-section laser beam, (outer diameter 35mm, inner diameter 15mm) was focused by a 500mm focal length mirror in cassegrainian configuration. The majority of the trials were carried out for workpiece distances beyond focus of 109, 69, 49 and 35mm (spot diameters 7.7, 4.8, 3.4 and 2.4mm) where the intensity distribution was annular. Most results are quoted in terms of a nominal applied power density (based on beam outer diameter only) and beam interaction time τ (beam outer diameter divided by scan speed); in all cases the beam power incident on the work was in the range 4.5-5kW, yielding nominal power densities 10,25, 50 and 100kW cm^{-2} corresponding to the above conditions. Scan speeds ranged from 2.8 to 67mms^{-1}. Samples were of different thickness (related to possible component applications) and were placed on a 10mm thick chill block, or on a hot-plate if pre-heat was required. Substrate surfaces were manually scoured with abrasive-coated nylon mesh before processing, particular care being taken with the tenacious oxide-forming nickel-base and aluminium-base alloys. Care was also taken to maintain helium cover at the interaction zone and for a distance of 100mm downstream of the sample movement. The additive powders were preplaced as a 1mm thick layer; for the work involving a number of adjacent scans, the powder was relaid between scans.

3. GENERAL FEATURES AND PROCESS CONDITIONS

The four combinations of substrate/coating were processed for a range of scan speeds and distances from focus. 'Geometrical' dilution was assessed from the cross-sectional area ratio (melt below original surface line/total

melt). The left hand part of Figure 1 shows data for deposition of Stellite 6 on cast iron, individual track conditions being shown by a circle within which is marked the geometric dilution. Circles enclosing the value zero indicate that negligible substrate melting has occurred, although a well-wetted, highly adherent coating may have resulted; this phenomenon was more common with the cast iron and steel substrates then with the aluminium and nickel alloys. The preferred operating region has: a right-hand boundary determined by insufficient energy input to cause substrate melting i.e. lack of wetting and bonding; a left-hand boundary chosen from dilution considerations; an upper boundary in the region of high beam intensity determined by the onset of excessive disruption of the melt, material vaporisation, and loss of additive; a lower boundary (low intensity) characterised by excessive bulk heating of the substrate. Shown in the Figure is a continuous line representing an energy density of $5kJcm^{-2}$, and a broken line representing constant, measured geometric dilution of approximately 10%. These two lines lie closely parallel, although the latter diverges at low intensity/long interaction time due to bulk heating. Inset in Figure 1 are the corresponding results for C, A and D. The lines of constant energy density shown for the first two are at $4kJ\ cm^{-2}$ and for the third (low melting point substrate) at $2kJ\ cm^{-2}$. Figure 2 shows a series of optimised adjacent tracks for each combination.

4. CHROMIUM CARBIDE ON NICKEL ALLOY (A)

For all conditions shown on the relevant inset in Figure 1, and provided good wetting was achieved, essentially pore-free, well bonded tracks were obtained. Detailed analysis was performed on tracks produced at $75kWcm^{-2}$ and interaction times in the range 0.07 to 0.14s. Figure 3 shows the cross sectional microstructures corresponding to the largest and smallest values of τ. For the shortest dwell time the bulk microstructure consisted of coarse angular Cr_3C_2 particles in a fine two phase matrix, whilst at the longest dwell time the microstructure consisted entirely of the two phase structure. For tracks produced at the fastest speeds, the hardness varied from 1400/1350HV0.5 at the crown down to 1070/1030 HV at the interface. For the more homogenous structures at the opposite end of the process range, the hardness varied from 1150/1100 HV down to an interfacial hardness of 870/810HV. Figure 4 shows typical results of concentration profiling across tracks processed at opposite ends of the treatment range. For smallest τ, the fluctuations in Ni and Cr reflect the presence of Cr_3C_2 particles, whilst the homogeneous layer of largest τ yields smoother profiles; iron was uniformly distributed, suggesting strong convection of the melt (1). Against the attractions of these high-hardness, low-porosity, well-bonded coatings must be set the high incidence of transverse cracking (typically every 2mm) associated with shrinkage stresses in the low-ductility layer. Signficant improvements resulted from choice of conditions yielding higher dilution (reducing hardness, increasing ductility), and from use of substrate preheat. There is scope for further investigation, and in the meantime, cracks had to be accepted in the wear test specimen.

5. STELLITE ON CAST IRON (B)

Figure 1 shows process conditions. Porosity was now encountered, probably due to substrate O_2, and a reducing reaction which liberated CO and/or CO_2. Preliminary indications are that it is minimised for low dilution and long interaction time (consistent with a chemical contribution from the

substrate, and with the time taken for bubbles to escape from the melt). The O_2 content of the substrate was ~ 0.015% so that a ~100μm thick layer could result in evolution of CO corresponding to 15% of the volume of the 1mm thick clad layer. The oxygen may of course be very inhomogeneously distributed, and Figure 5 shows the results of separate investigations in which it was predominantly associated with the graphite flakes. The cladding parameters were 25kW cm^{-2}, 12mm s^{-1}. The surface oxygen level of the substrate was first locally enhanced by an 11mm wide laser transformation hardening pass in air (colloidal graphite absorber, no melt, applied power density 6.0kW cm^{-2}, τ = 0.19s). Analysis of a surface layer 1mm thick indicated that in this scan, the average oxygen content had risen to approximately 0.05%. A Stellite track was then deposited, the scan direction lying at right-angles to the hardening scan. Figure 5a shows the region of intersection of the two tracks, with the associated localised evolution of gas at the zone of higher oxygen content. Figure 5b confirms this in the longitudinal section, and Figure 5d shows that the pores have 'grown' from the graphite flakes. The likely explanation is seen in the micrograph at Figure 5c; oxide layers are present on the matrix around graphite flakes which were exposed at the original surface. Away from the region of prior heat treatment, the track is largely pore-free as seen in Figure 5e. The underlying transformation hardened band (~ 800HV max) is ill-suited to withstand shrinkage stresses and small edge cracks may appear (Figure 7). The preliminary evidence is that cracking is more prevalent for full convex profiles rather than flat beads, and if imperfect gas shrouding permits formation of oxides along the graphite network. The problem does not seem to arise for higher ductility coatings such as Colmonoy 26 (350HV) a nickel-base alloy designed for use on cast iron. Experimental isochronal annealing of clad samples was carried out for 2 hours with the results shown in Figure 6. In the untempered condition, coarse acicular martensite, filamentary ledeburite and retained austenite were present at the interface, but after the 650°C temper, the retained austenite and primary austenite dendrites transformed to ferrite and carbide whilst the fine ledeburitic carbide remained relatively unaffected. An example of a clad Stellite edge (after machining) is shown in Figure 8. A preformed groove located the powder, and subsequent machining removed any incipient edge cracks. No transverse cracks were observed in the specimen which had a length of 40mm.

6. STELLITE ON STRUCTURAL STEEL (C)

Cladding here was straightforward and pore-free. The low carbon (~ 0.2%) substrate yielded transformed maximum hardness under the coating of typically 350-400HV. The upper inset in Figure 1 shows the range of investigation, and it is seen that for a number of conditions at 10 and 25kW cm^{-2} there is nominally zero dilution. All of these (with the exception of the longest τ case) exhibited good wetting and adhesion. Moving to use of 50kW cm^{-2} permitted good control of coating dilution and a series of runs at different scan speeds was performed in which average hardness, dilution and ductility of the tracks were assessed. The ductility was gauged by a three-point tensile bend test applied to a sample strip having a 40mm long clad track; the deflection (enabling calculation of elongation) which caused formation of a single transverse crack was noted. As τ increased from 0.10 to 0.23s, dilution increased from 1.4 to 19.6%, hardness fell from 530 to 454HV, and elongation before cracking increased from 0.16 to 2.8%.

7. SILICON ON ALUMINIUM (D)

The lower inset in Figure 1 indicates the generally larger dilution observed in this combination,the highest values appearing at low intensity. Figure 9 shows, left to right, macrographs and micrographs of tracks created with 50kW cm^{-2} for τ = 0.051, 0.061 and 0.082s (67, 56 and 42mm s^{-1}). The structures consist of silicon particles (980HV) embedded in an Al Si eutectic matrix. The microdendrites in the recast substrate zone ensured good mechanical keying. The brief heating cycle has prevented segregation of magnesium with possible formation of brittle β phase at grain boundaries. Figure 9a shows that in the lowest τ case there has been insufficient energy input for the eutectic matrix to adequately form and totally encase the silicon particles. Angular voids with scale length typically 20μ result, and they randomly occupy 6% of the cladding. Whilst these voids must inherently degrade mechanical properties, they could act as sites for lubricant retention. Higher τ (Figure 9b and 9c) resulted in disappearance of the voids. The secondary electron images and corresponding X-ray maps of the structures near the crown (Figure 10) confirm that increase in τ results in reduction of primary Si particle content and corresponding increase in Al; compositional dilution was measured to be 21% and 49% for small and large τ respectively. Figure 11 shows results for the three scan conditions, and it is seen that hardness and volume fraction of primary silicon increase with scan speed, whilst melt depth and dilution decrease. Experimental solution treatment and/or ageing (at 155°C) of the tracks yielded no improvement in final hardness. For example, ageing of the as-deposited tracks (332HV) at 155°C for 3, 4 or 5 hours yielded final hardnesses of 317, 317 and 303HV (typical errors ± 7HV) respectively.

8. WEAR TESTING

The chromium carbide/nickel alloy sample A (25kW cm^{-2}, τ = 0.25s) and the silicon/aluminium alloy sample D (50kW cm^{-2}, τ = 0.057s) of Figure 2 were ground flat and their wear resistance evaluated using a reciprocating pad-on-plate technique (8). Comparison was made with the performance of flame-sprayed chromium carbide and untreated aluminium alloy, respectively. The wear rates, expressed as depth removed per pass are shown in Figure 12. It is seen that laser-deposited Cr_3C_2 shows a reduction in wear rate to approximately one third that seen in a flame-sprayed coating; furthermore the effect of silicon enhancement by laser is to reduce wear rate to approaching one quarter the level seen with the untreated substrate.

9. CONCLUSIONS

This work demonstrates that cladding with laser power of 4½-5kW (a level at which there is an increasing choice of industrial lasers) can be carried out very effectively using (a) the defocused, annular output beam from an unstable resonator (b) preplaced powder, which could equally well have been supplied just ahead of the beam (gas borne or under gravity from a vibrating reservoir) (c) careful gas shielding. For a 1mm thick powder layer in the combinations studied, typical energy input values to avoid excessive dilution are: 4kJ cm^{-2} for Cr_3C_2/Ni alloy (A); 5kJ cm^{-2} for Stellite/cast iron (B); 4kJ cm^{-2} for Stellite/steel (C); 2kJ cm^{-2} for silicon/aluminium alloy (D). For combination A dilutions of 15-20% are routinely achieved; cracking is a problem although pre-heat (not described here) helps significantly. Tracks (without preheat) exhibit an approximately three-fold increase in wear performance compared to commercially flame-sprayed tracks

of the same material. Combination B is prone to the formation of pores and cracks, although long interaction times, low dilutions and low substrate O_2 content are found to be beneficial. Edge cracks which develop because of shrinkage stresses are prevented by selecting coatings with good ductility. Stress relieving of the substrate after cladding does not affect the properties of the cladding. With combination C, low dilution, pore-free cladding is readily achieved. In combination D, the range of routine dilution (25-60%) is significantly higher than with the other combinations because of the high melting point difference between silicon and aluminium alloy. Nevertheless dilution control within the range is good. The mechanical strength properties of as-deposited tracks cannot be improved by further heat-treatment. The wear performance of a laser-treated track with average dilution in the above range is typically approximately four times better than the non-heat-treatable parent substrate material. In broad terms, the results provide further evidence of the precision and controllability of the process. Whilst discussion of economics is outside the scope of the paper, we believe that the work affirms the strong industrial potential of the process.

10. ACKNOWLEDGEMENTS

We much appreciate the active interest and support of A.S. Kaye, I.J. Spalding, B.A. Ward and other colleagues of the Culham Laboratory Laser Applications Group. The analytical work of A. Green (Liverpool University) and the experimental assistance of P.M. McElroy (formerly of Liverpool University) is gratefully acknowledged

11. REFERENCES

(1) Belmondo A. and Castagna M., 'Wear-resistant coatings by laser processing', Thin solid films Vol 64, (1979) 249-256.

(2) Gnanamuthu D.S., 'Laser surface treatment', Proc. Conf. Applications of lasers in Materials Processing', pp177-212 ed. E.A. Metzbower Washington 18-20 April 1979. A.S.M. Ohio.

(3) Ayres J.D., Schaefer R.J. and Robey W.P., 'A laser processing technique for improving the wear resistance of metals', Journal of Metals, August 1981, pp 19-23.

(4) Megaw J.H.P.C. and Kaye A.S., 'High power lasers and laser metalworking' 4th European Electro-Optics Conf., Utrecht, Proc. Soc. Photo-Optical Instrumentation Engineers, Vol. 164, 241-251.

(5) Steen W.M. and Courtney C.G.H., 'Hardfacing of Nimonic 75 using 2kW cw CO_2 laser', Metals Technology, June (1980) pp232-237.

(6) Powell J. and Steen W.M., 'Vibro laser cladding', Proc. Trans. Met. Soc. Annual Meeting, AIME Conference, Chicago, Feb 1982, pp 93-104.

(7) Walther H. and Pera L., 'A high power laser metal working facility and its applications', Ibid Ref (4) pp 252-270.

(8) Trafford D.N.H., Bell T., Megaw J.H.P.C. and Bransden A.S., 'Laser treatment of grey iron', Metals Technology, Vol 10, 2 (1983).

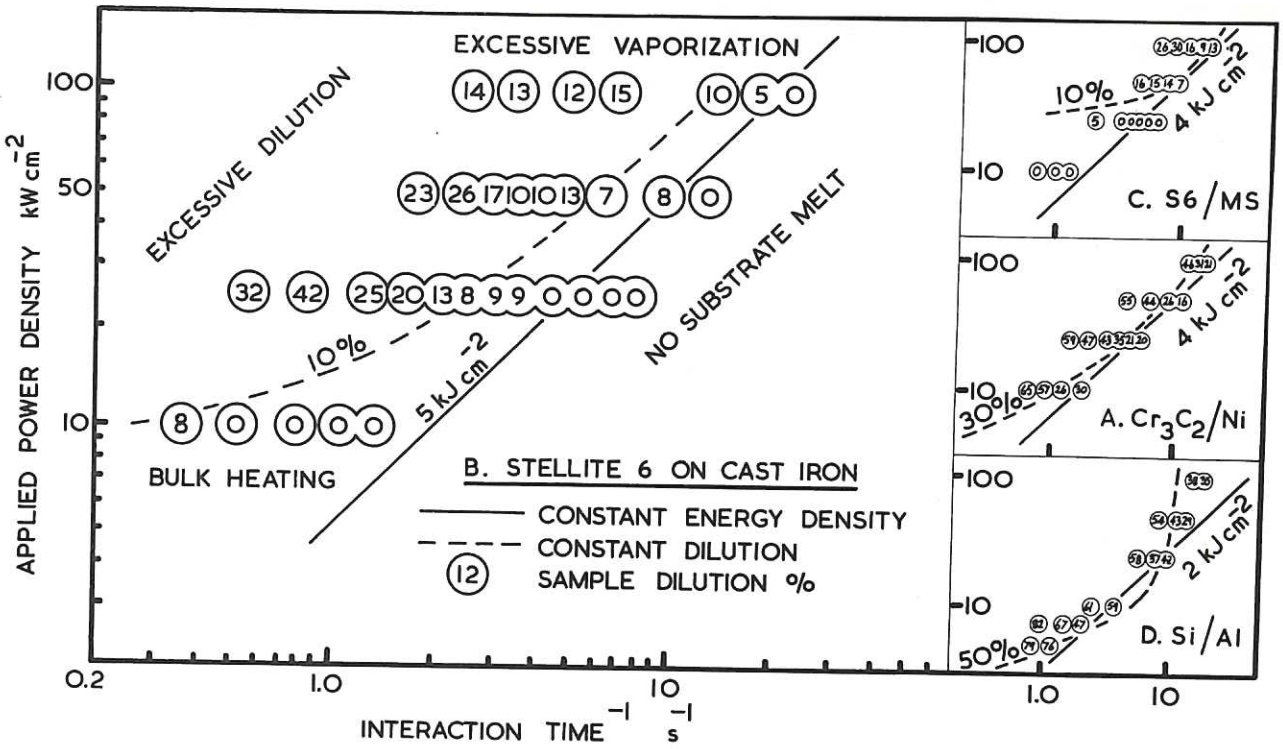

Fig.1 Process conditions for four combinations of coating/substrate.

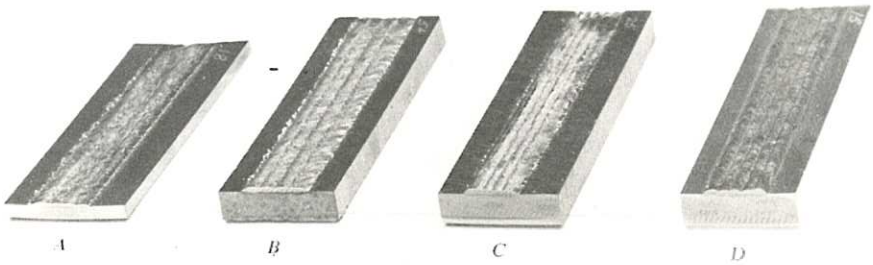

Fig.2 Samples (in each combination) clad with adjacent passes.

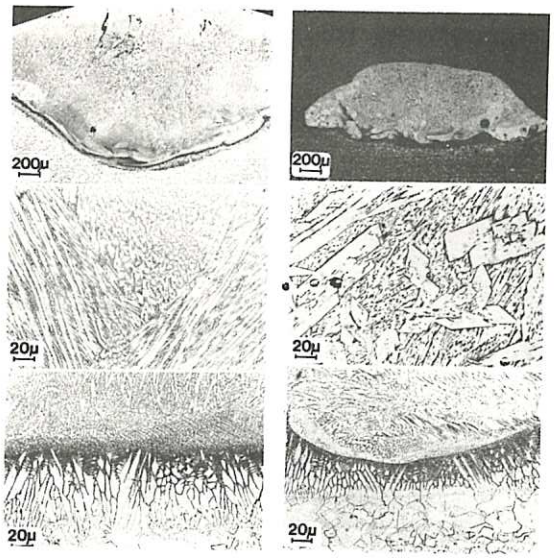

$\tau = 0{\cdot}14$ s $\tau = 0{\cdot}07$ s

Fig.3 Cr_3C_2 tracks–see text.

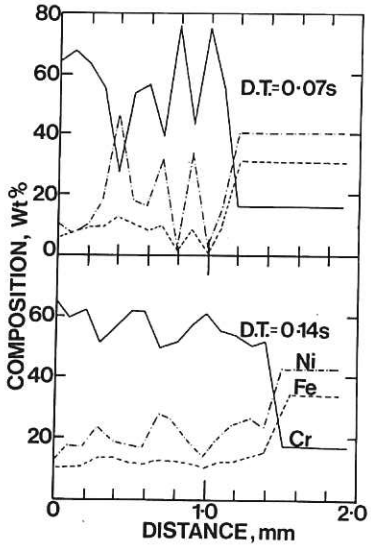

Fig.4 Profiles of concentration for Cr_3C_2.

CLM-P699

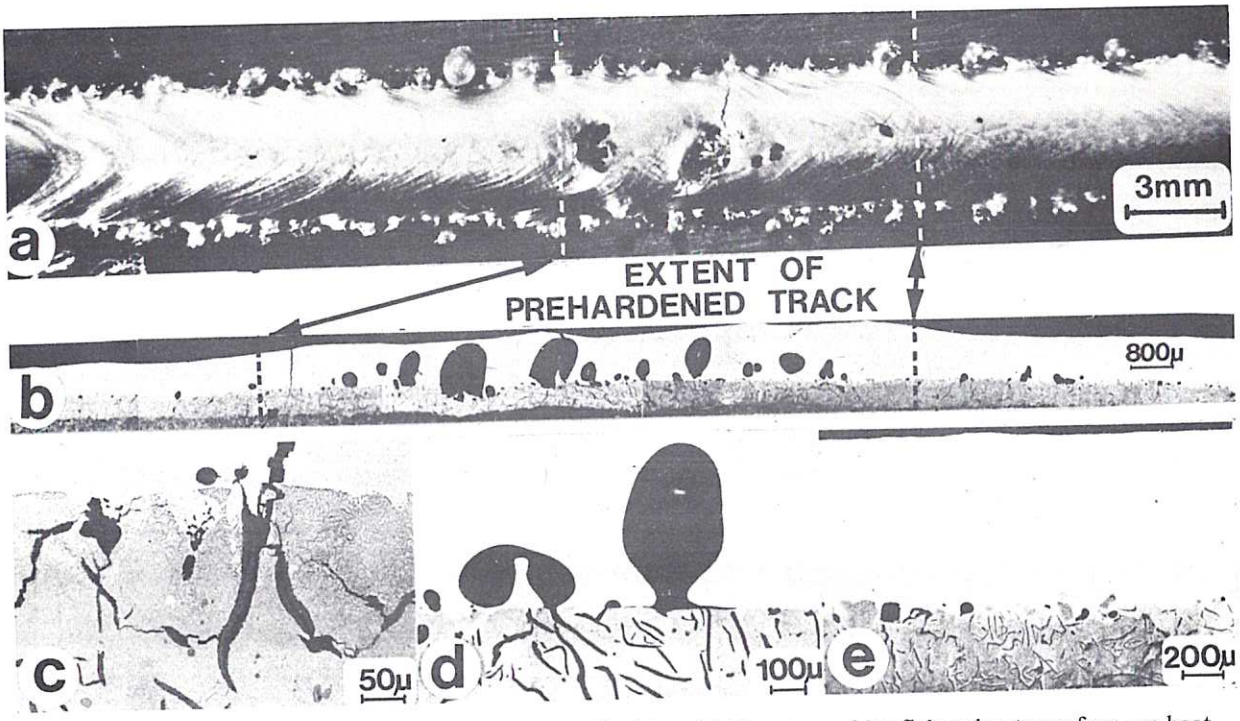

Fig.5 Stellite track on cast iron—porosity associated with oxidation at graphite flakes due to surface pre-heat.

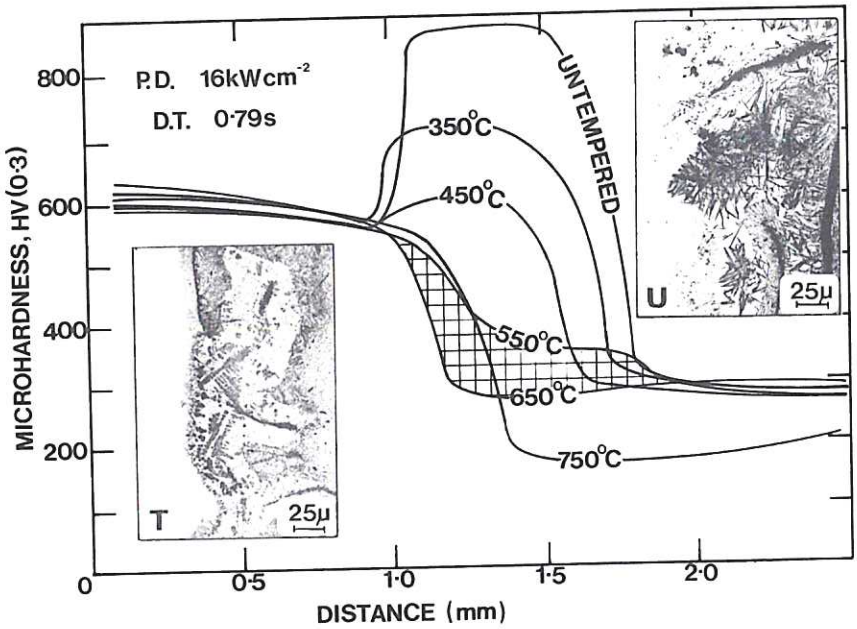

Fig.6 Effect of tempering on hardness and structure for Stellite on cast iron.

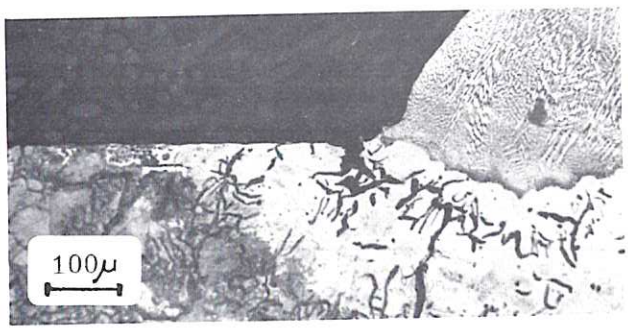

Fig.7 Edge crack in cast iron.

Fig.8 Stellite-clad edge.

CLM-P699

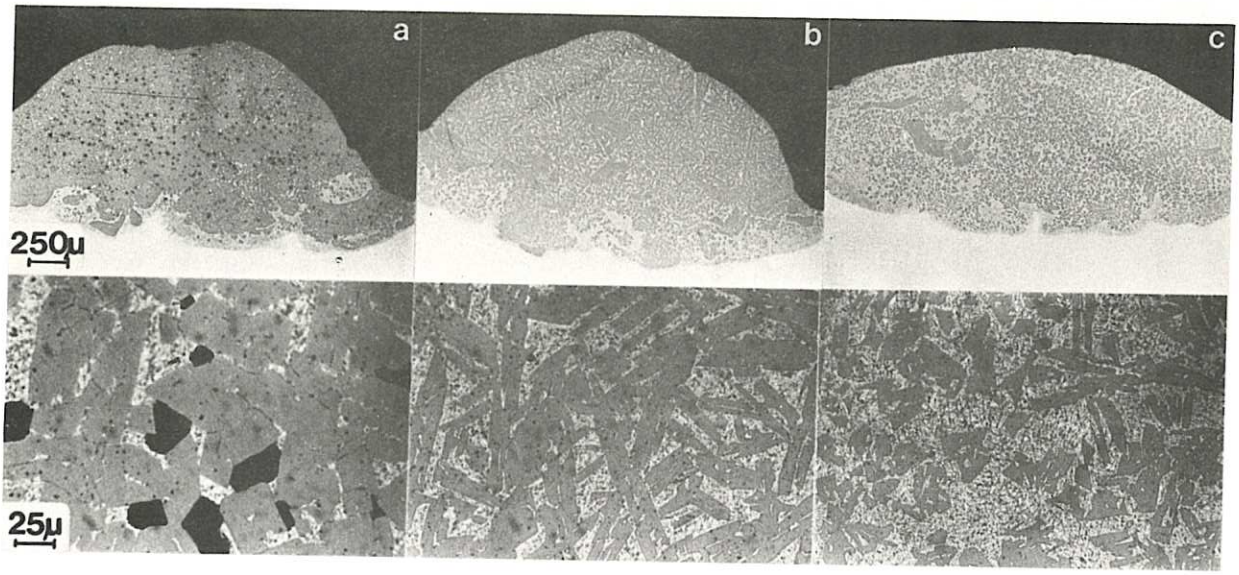

Fig.9 Si on Al alloy—dilution increasing with interaction time.

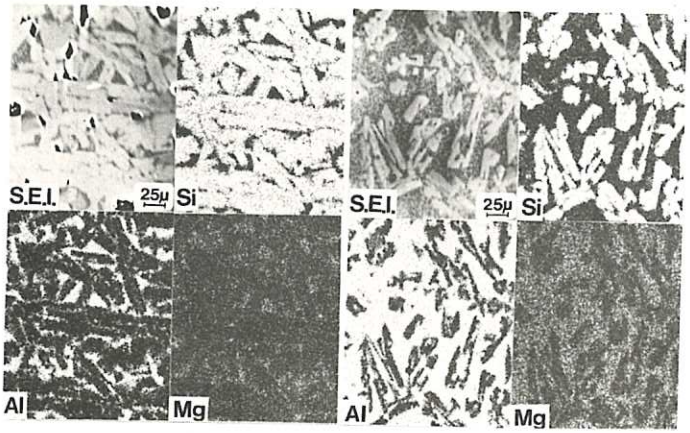

$\tau = 0{\cdot}051$ s $\tau = 0{\cdot}082$ s

Fig.10 SEI and X-ray maps—Si on Al alloy.

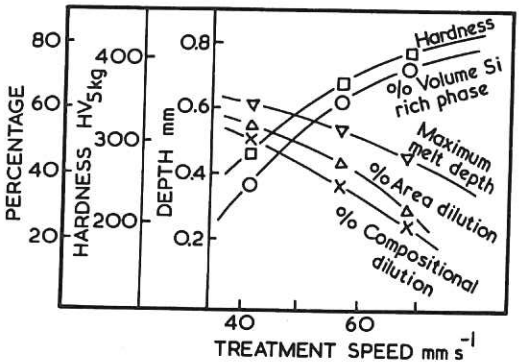

Fig.11 Variation of properties with scan speed for Si on Al alloy.

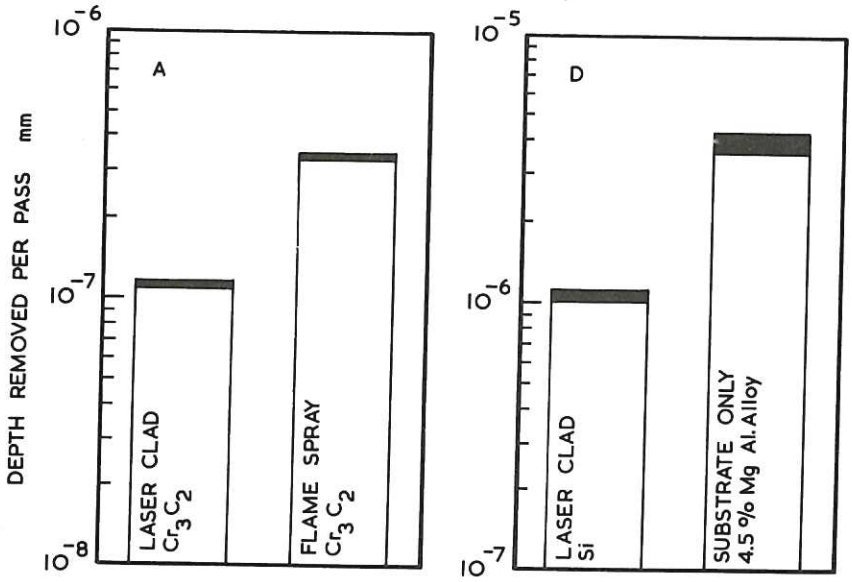

Fig.12 Wear performance data.